Shear flow suppression of turbulent transport and self-consistent profile evolution within a multi-scale gyrokinetic framework

M. Barnes 1,2), F. I. Parra 1), E. G. Highcock 1,2), A. A. Schekochihin 1), S. C. Cowley 2), and C. M. Roach 2)

1) Rudolf Peierls Centre for Theoretical Physics, University of Oxford, Oxford, UK
2) EURATOM/CCFE Fusion Association, Culham Science Centre, Abingdon, UK

E-mail contact of main author: michael.barnes@physics.ox.ac.uk

Abstract. The turbulent heat and momentum fluxes obtained from local, nonlinear gyrokinetic simulations with mean toroidal flow are presented. The behavior of the fluxes are characterized by scans in temperature and flow gradient for both zero and finite magnetic shear. Linearly unstable eigenmodes are absent for sufficiently large flow shear, but transient linear growth is found to drive subcritical turbulence whose amplitude increases with flow shear. Consequently, the heat fluxes are minimized at a finite flow shear. By considering the intersection of contours of heat flux (or injected power) and the ratio of momentum to heat flux (inversely proportional to beam energy), bifurcations in the temperature and flow gradients are observed. An analysis is presented showing when such bifurcations are possible and how large the jumps in gradient can be. This zero-dimensional analysis is then extended to the one-dimensional case using the multi-scale transport solver, `TRINITY`. Using model turbulent fluxes, the plasma performance is found to be optimized at a finite value for the ratio of applied torque to power.

1 Introduction

It is well known that the performance of fusion devices is limited by heat fluxes arising from small-scale turbulence driven by large-scale profile gradients. The presence of this turbulence is not inevitable, as demonstrated by the formation of transport barriers in H-mode and advanced scenario discharges in a wide range of experimental devices. The details of how these transport barriers are triggered and saturated vary from case to case, but a common feature is the favorable role played by mean $\mathbf{E} \times \mathbf{B}$ flow shear and zero or negative magnetic shear in providing steeper temperature gradients [1, 2]. Consequently, it is of great interest to determine how localized regions of strong $\mathbf{E} \times \mathbf{B}$ flow shear can develop and the extent to which this flow shear can suppress turbulent transport.

Previous numerical studies of the effect of mean flow shear on turbulence have found that the shear in the $\mathbf{E} \times \mathbf{B}$ component of the flow is stabilizing and can, in some cases, fully quench turbulent transport [3, 4, 5]. However, the shear in the parallel flow (henceforth referred to as the parallel velocity gradient, or PVG) has been shown to drive linear instability [6, 7]. Since the flow is constrained to be purely toroidal in the limit of large flow velocity (of order the ion thermal speed), the relative importance of the $\mathbf{E} \times \mathbf{B}$ and parallel velocities is set by the ratio of the poloidal to toroidal magnetic field [8]. The turbulent transport is thus not always fully quenched and may increase with flow shear [5].

In this paper, we present new theoretical and numerical results on the effect of flow shear on turbulence and on the subsequent evolution of the macroscopic profiles over the confinement time scale.

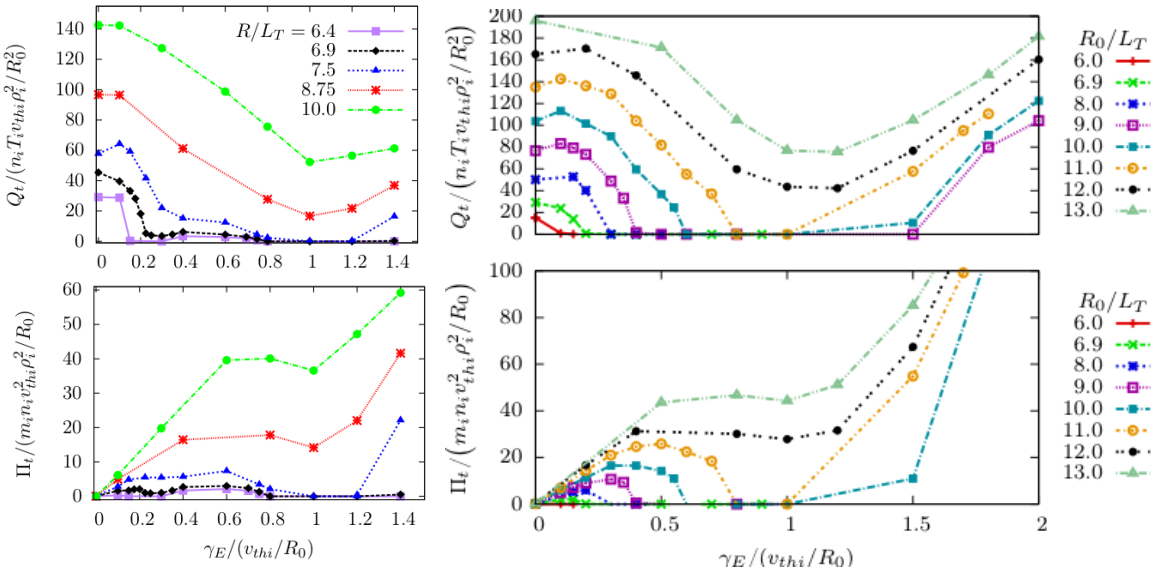

Figure 1: Gyro-Bohm normalized turbulent heat (top) and momentum (bottom) fluxes vs shearing rate for different temperature gradient scale lengths. Fluxes on left correspond to $\hat{s} = 0.8$ (figures taken from [11]) and those on right to $\hat{s} = 0$ (figures taken from [12]).

2 Turbulent heat and momentum fluxes in the presence of mean flow shear

To determine the properties of turbulent fluxes in the presence of mean flow shear, we conducted a series of nonlinear simulations using the gyrokinetic flux tube code `GS2` [9]. The magnetic geometry corresponds to the Cyclone base case [10], with varying values of the inverse temperature gradient scale length, R/L_T, and the $\mathbf{E} \times \mathbf{B}$ flow shearing rate, $\gamma_E = (r/q)(d\omega/dr)$, as well as two values of magnetic shear, $\hat{s} = d\ln q/d\ln r = 0.8$ and 0. The key results from these simulations are given in Figs. 1-3 and 6.

The turbulent momentum and heat fluxes for the zero magnetic shear [12] and finite magnetic shear ($\hat{s} = 0.8$) [11] cases are qualitatively similar (Fig. 1), but quantitatively the $\hat{s} = 0$ case has better transport properties. For sufficiently large R/L_T, the heat flux decreases to a minimum around $\gamma_E = v_{thi}/R$ before increasing monotonically. For a given R/L_T, this minimum is lower for the $\hat{s} = 0$ case, but it occurs at approximately the same γ_E. The momentum flux increases from zero to a local maximum, followed by a local minimum around $\gamma_E = v_{thi}/R$ and subsequent increase. The turbulent Prandtl number, $\mathrm{Pr}_t = \nu_t/\chi_t$, with $Q_t = -\chi_t dT_i/dr$ and $\Pi_t = -\nu_t m_i R_0 (qR_0/r)\gamma_E$, is given in Fig. 2. For moderate to large γ_E, Pr_t is order unity and approximately independent of R/L_T and γ_E. Its variation at small γ_E is consistent with the "$\mathbf{E} \times \mathbf{B}$ shear pinch" discussed in Ref. [13].

For both values of $\hat{s}$, the turbulence for $\gamma_E \gtrsim v_{thi}/R$ is subcritical (no linearly unstable eigenmodes) and is a result of transient growth driven by the PVG [14]; for the $\hat{s} = 0$ case, all growth is transient [15]. Amplification factors for the transient growth increase with γ_E beyond $\gamma_E \sim v_{thi}/R$, as shown in Fig. 3. This transient amplification is not a result of Floquet oscillations: it is driven by the PVG (and is thus found in a slab geometry, as shown in Ref. [14, 15]). Furthermore, this PVG-driven turbulence is not to be confused with the increase in fluxes arising from linearly unstable eigenmodes driven by the PVG [5, 8] (seen for $R/L_T = 6.4$ and 6.9 at $\gamma_E \approx 0.4 v_{thi}/R$ in Fig. 1), which we

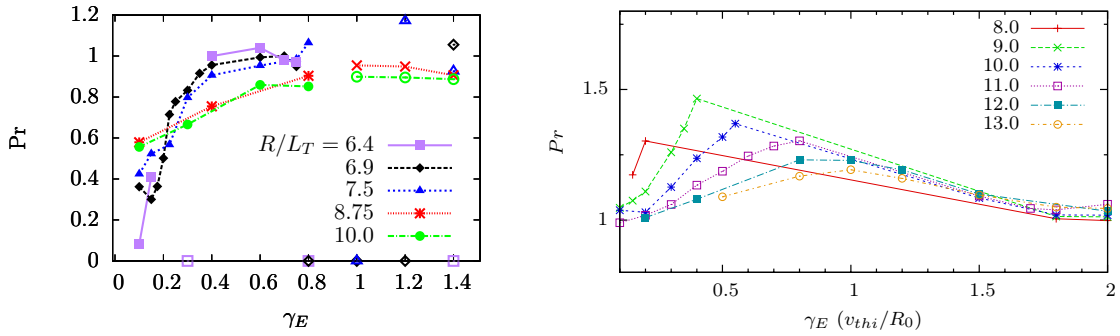

Figure 2: Turbulent Prandtl number for $\hat{s} = 0.8$ (left, [11]) and $\hat{s} = 0$ (right). For moderate to large γ_E, Pr_t is approximately independent of γ_E and R/L_T.

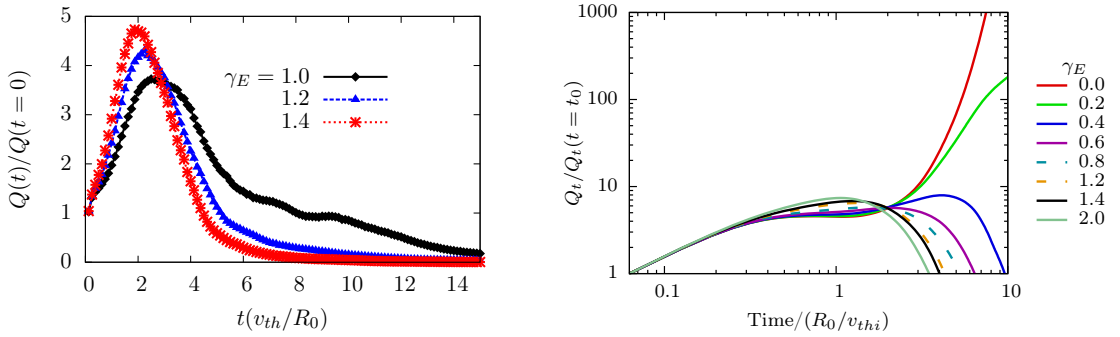

Figure 3: Turbulent heat flux (normalized to its initial value) vs. time for $\hat{s} = 0.8$ (left, [11]) and $\hat{s} = 0$ (right, [12]). For sufficiently large γ_E, transient amplification factor increases with flow shear.

find are stabilized by sufficiently large γ_E.

3 Bifurcations in temperature and flow gradients: 0D analysis

Thus far we have determined the turbulent fluxes associated with given values of R/L_T and γ_E. We now consider the inverse problem, in which we predict R/L_T and γ_E for given values of the input heat and momentum. In order to gain an understanding of what types of solutions are possible, we first employ a simple model for the heat and momentum fluxes [16] designed to reproduce the qualitative behavior exhibited in our simulations. The Gyro-Bohm normalized heat flux is approximated as offset linear:

$$Q_t = \chi_t \left[\frac{R}{L_T} - \frac{R}{L_{Tc}}(\gamma_E) \right] \tag{1}$$

where

$$\frac{R}{L_{Tc}}(\gamma_E) = \frac{\alpha \gamma_E R_0 / v_{thi} + \kappa}{1 + \alpha \gamma_E^2 / (\alpha + 2\kappa)} \tag{2}$$

is the γ_E-dependent critical temperature gradient scale length. Here κ is $R/L_{Tc}(\gamma_E = 0)$, and α and χ_t are free parameters, which we specify to best fit the results of the $\hat{s} = 0$ case (chosen because it has favorable transport properties relative to the $\hat{s} = 0.8$ case). Curves showing Q_t as a function of γ_E for different values of R/L_T are given in Fig. 4.

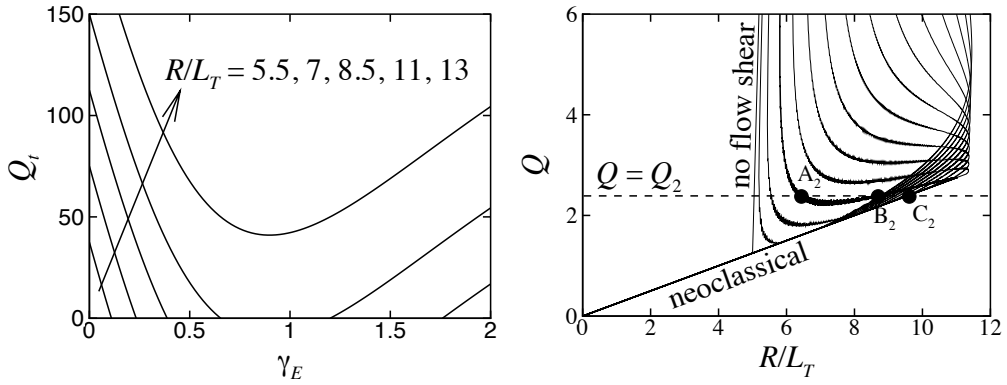

Figure 4: (Left): Illustration of the simple model (Eqs. (1)-(2)) used for turbulent heat flux. Compare with upper right panel of Fig. 1. (Right): Contours of constant Π/Q (normalized to Gyro-Bohm fluxes) arising from the model. Increasing Π/Q corresponds to moving towards the top right of the figure. The dashed line represents a heat flux value for which there are three solutions for R/L_T. Both plots from Ref. [16].

The Gyro-Bohm normalized turbulent momentum flux is specified in terms of Q_t through Pr_t:

$$\Pi_t = -\mathrm{Pr}_t \frac{R}{v_{thi}} \frac{\gamma_E}{R/L_T} \frac{qR}{r} Q_t. \tag{3}$$

Based on the results presented in Fig. 2, we take Pr_t to be a constant value of approximately unity. The total heat and momentum fluxes (Gyro-Bohm normalized) are given by the sum of the turbulent and neoclassical contributions: $Q = Q_t + Q_n$ and $\Pi = \Pi_t + \Pi_n$. While the neoclassical contributions are typically small, they are often comparable to the turbulent ones in transport barriers. We find that they are necessary (in the absence of any other flux contributions) to obtain transport bifurcations.

The solutions for R/L_T and γ_E corresponding to given values of Q and Π/Q (labeling injected power and beam energy, respectively) are shown in Figs 4 and 5. From Fig. 4 we see that for a range of values of Q and Π/Q, multiple solutions for R/L_T exist. This is understood by considering the contours of constant Q and Π/Q in the (R/L_T,γ_E) plane, given in Fig. 5. Far above (below) the $R/L_{Tc}(\gamma_E)$, the fluxes are dominated by turbulent (neoclassical) contributions. In these regions of parameter space, Eq. (3) and an analogous equation for the neoclassical fluxes indicate that Π/Q contours will be straight lines whose slopes depend on the Prandtl number. Since the neoclassical Prandtl number, Pr_n, is typically much smaller than Pr_t, the slope of the Π/Q curves will be smaller in the neoclassical dominated region than in the turbulence dominated region. The neoclassical heat flux is independent of γ_E, and thus constant-Q curves are horizontal lines for $R/L_T < R/L_{Tc}$. For $R/L_T \gg R/L_{Tc}$, $Q \approx Q_t$, which from Eq. (1) gives constant-Q curves with the same shape as the curve of R/L_{Tc}. In the narrow region of parameter space surrounding the R/L_{Tc} curve, the neoclassical and turbulent contours join smoothly.

Intersections of the constant Q and Π/Q curves give the local solutions for R/L_T and γ_E. For large (small) Q, the fluxes are purely turbulent (neoclassical) and there is only one intersection with the straight Π/Q constant line. In the region where $Q_t \sim Q_n$, the Π/Q constant curve is no longer a straight line, and it is possible to have two or three intersection points. The curve $Q = Q_2$ in Fig. 5 with three intersections cor-

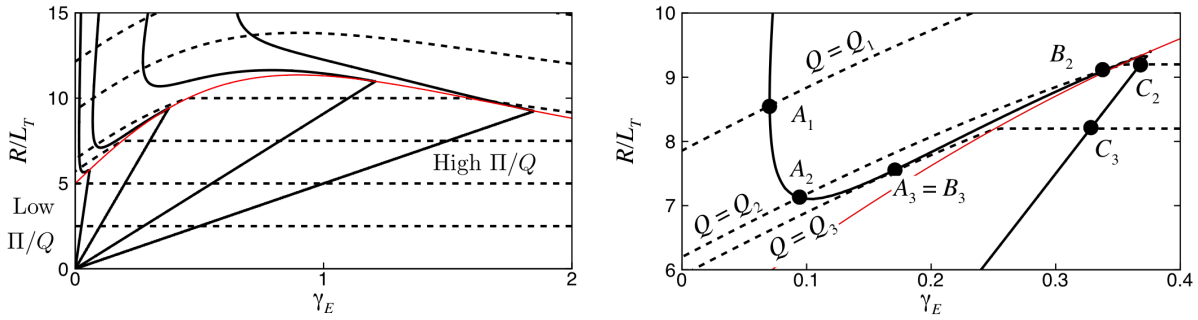

Figure 5: Curves of constant Q (dashed lines) and Π/Q (solid lines), with the R/L_{Tc} given by the red line. The decrease in R/L_{Tc} for $\gamma_E \gtrsim 1$ is a result of PVG-driven subcritical turbulence. Intersections of the solid and dashed lines correspond to solutions of the system. The plot on the right shows either one ($A1$), two ($A3, C3$) or three ($A2, B2, C2$) solutions are possible depending on the value of Q. Both plots from Ref. [16].

responds to the three solutions for R/L_T shown in Fig. 4. The criterion for having multiple solutions is $(d(R/L_T)/d\gamma_E)_Q \leq (d(R/L_T)/d\gamma_E)_{\Pi/Q}$ in the vicinity of R/L_{Tc}, where the subscript on the derivatives indicates the quantity held fixed. Expanding in $(R/L_T - R/L_{Tc}) \sim \chi_n/\chi_t \ll 1$, it can be shown that the approximate criterion for multiple solutions is [16]

$$\frac{d(R/L_{Tc})}{d\gamma_E} \geq \frac{1}{\mathrm{Pr}_t}\frac{\Pi}{Q}\frac{r}{qR}\frac{v_{thi}}{R}\left(\frac{R/L_{Tc}}{\gamma_E}\right)^2 > \frac{qR}{r}\frac{\mathrm{Pr}_n^2}{\mathrm{Pr}_t}\frac{R}{v_{thi}}\left(\frac{\Pi}{Q}\right)^{-1}, \tag{4}$$

where the second inequality follows from Eq. (3) and its neoclassical analog (along with the assumption $\mathrm{Pr}_n < \mathrm{Pr}_t$).

From the second inequality in Eq. (4), it is evident that bifurcations are not possible for Π/Q too small. There is also an upper bound on Π/Q, obtained by rearranging the first inequality of Eq. (4). Consequently, bifurcations are possible only in a limited window in Π/Q. The necessary, but not sufficient, condition for bifurcations is [16]

$$\frac{\mathrm{Pr}_n^2}{\mathrm{Pr}_t}\frac{qR}{r}\frac{R}{v_{thi}}\left(\frac{d(R/L_{Tc})}{d\gamma_E}\Big|_{\gamma_E=0}\right)^{-1} < \frac{\Pi}{Q} \leq \mathrm{Pr}_t\frac{qR}{r}\frac{R}{v_{thi}}\left(\frac{\gamma_{E,max}}{R/L_{Tc,max}}\right)^2\frac{d(R/L_{Tc})}{d\gamma_E}\Big|_{\gamma_E=0}, \tag{5}$$

where $R/L_{Tc,max}$ is the maximum value of R/L_{Tc}, $\gamma_{E,max}$ is the corresponding γ_E, and we have assumed $d^2(R/L_{Tc})/d\gamma_E^2 < 0$ so that $d(R/L_{Tc})/d\gamma_E$ is largest at $\gamma_E = 0$. This interval is shifted to lower (higher) Π/Q values by decreasing (increasing) qR/r. It is widened by decreasing Pr_n and increasing $d(R/L_{Tc})/d\gamma_E$ (i.e. enhancing suppression of turbulence, as in the case of zero magnetic shear). Using approximate values taken from the $\hat{s} = 0$ simulations ($\mathrm{Pr}_n \approx 0.1$, $\mathrm{Pr}_t \approx 1$, $qR/r \approx 8$, $\gamma_{E,max} \approx v_{thi}/R$, $R/L_{Tc,max} \approx 11$, $d(R/L_{Tc})/d\gamma_E|_{\gamma_E=0} \approx 5R/v_{thi}$), we get $0.016 < \Pi/Q \leq 0.331$.

We now return to the nonlinear gyrokinetic simulations for $\hat{s} = 0$ and consider contours of constant Q and Π/Q. These contours are formed by interpolating our large data set using radial basis functions with a linear kernel [17]. The results [12] are shown in Fig. 6. For the range of Π/Q values considered, there are multiple solutions for R/L_T and γ_E for a range of fixed Q and Π/Q values. Thus bifurcations exist in which significant shifts in R/L_T are found (for the case considered in Fig. 6, a shift of about fifty percent).

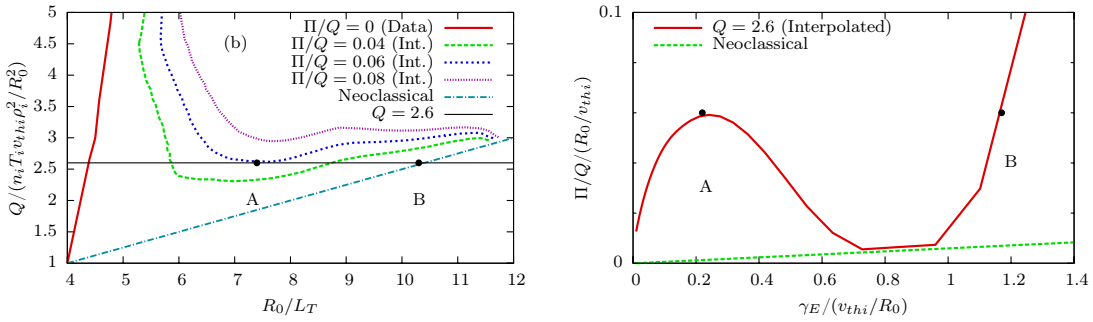

Figure 6: (Left): Contours of constant Π/Q show bifurcations in R_0/L_T as Q is varied. Cf. right panel of Fig. 4. (Right): Contour of constant Q shows bifurcation in γ_E as Π/Q is varied. Note that T is assumed constant. Both plots from Ref. [12].

4 1D transport model

Ultimately, we want to predict the self-consistent evolution of radial plasma profiles as they interact with the turbulence. Because of the enormous range of space-time scales involved and the high dimensionality of the problem, resolved first-principles simulations of the full core volume over the confinement time are very challenging using conventional techniques. To address this problem, we use the gyrokinetic transport solver `TRINITY` [18], which employs a multi-scale model [19, 20] that arises from the δf gyrokinetic ordering. By assuming a separation in space and time scales between the turbulence and the plasma profiles (generally valid for small-ρ_* devices), we obtain separate (coupled) equations describing their evolution. The fluctuation equations are then solved locally on the turbulence time scale, and the resulting ensemble-averaged fluxes are input in the equilibrium equations, which are solved globally on the confinement time scale. This amounts to coupling multiple flux tube simulations at different radii through the transport equations to obtain self-consistent plasma profiles and corresponding turbulent fluxes. Results from `TRINITY` simulations with nonlinear fluxes calculated by the gyrokinetic turbulence codes `GS2` and `GENE` are in reasonable quantitative agreement with L-mode and H-mode discharges on JET and ASDEX Upgrade [18].

Here, we present results from `TRINITY` simulations using the model turbulent fluxes described by Eqs. (1) and (3). These results are intended to provide a qualitative picture of fusion performance in devices with neutral beam injection of momentum and energy. Concentric, circular flux surfaces are used, with a flat safety factor profile (and thus $\hat{s} = 0$ everywhere, so that our turbulent flux model should be a good approximation). Energy and toroidal angular momentum are injected externally using a Gaussian deposition profile centered at the magnetic axis with a half-width of one-tenth the minor radius. The angular momentum and ion temperature are fixed at the outer boundary of the simulation domain (80% of the minor radius) to zero and 100 eV, respectively. A series of simulations were run in which the total input power and beam energy were varied over a wide range.

The key result is given by Fig. 7, which shows the central ion temperature T_0 as a function of the ratio of injected torque, τ_ϕ, to power, P_{in}, for a range of P_{in}. We have switched from Gyro-Bohm normalized Π/Q to τ_ϕ/P_{in} because the Gyro-Bohm normalization is a function of temperature, which varies radially in our 1D model. In order to make connection with the 0D results, we also present in Fig. 7 a plot of normalized Π/Q at mid-radius for

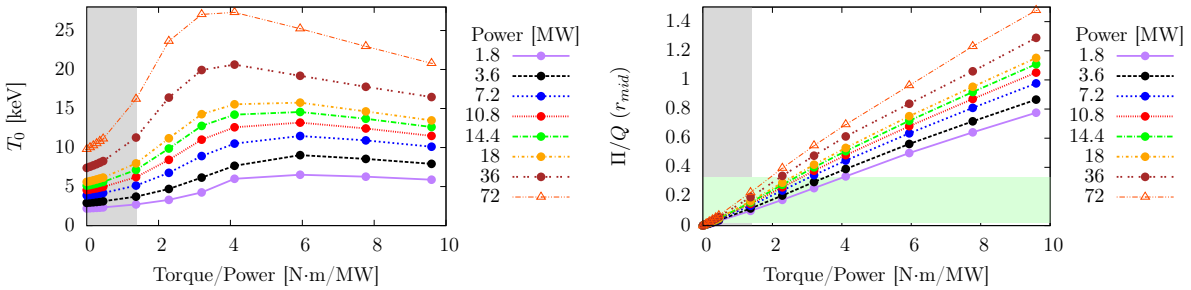

Figure 7: Central temperature (left) and Gyro-Bohm normalized Π/Q at mid-radius (right) vs. ratio of external torque to power for a range of input powers. The optimal ratio shifts to lower values as power is increased. Gray shaded region corresponds to accessible torque to power ratios on JET [21]. Green shaded region corresponds to Π/Q range satisfying approximate necessary condition for bifurcation (Eq. (5)).

each of our simulations. Increasing τ_ϕ/P_{in} from zero (at fixed P_{in}) initially results in larger T_0, as more momentum is being injected and thus larger flow shears are achieved. However, as the flow shear gets very large, the PVG-driven subcritical turbulence increases transport, so T_0 decreases with increasing τ_ϕ/P_{in} for large τ_ϕ/P_{in}. The maximum T_0 is thus achieved at a finite value of τ_ϕ/P_{in}, which decreases with increasing power. Thus increased beam power leads to an increase in T_0 not only due to more injected energy, but also because the optimal flow shear for confinement is achieved at smaller τ_ϕ/P_{in} (which is closer to where many modern fusion experiments operate [21, 22]).

5 Summary and discussion

Nonlinear gyrokinetic simulations have been used to identify transport bifurcations, in which the temperature gradient and rotational flow shear have multiple solutions for given values of Q and Π/Q. These bifurcations require finite neoclassical transport and exist in the absence of any external mechanisms, such as proximity to low order rational magnetic surfaces or coupling to MHD modes. The conditions under which such bifurcations exist were derived, showing that they are only possible within a limited range of Π/Q values. The jumps in R/L_T and γ_E associated with the bifurcation were found to be limited in some cases by the existence of subcritical turbulence driven by shear in the parallel component of the mean toroidal flow velocity.

Preliminary results from the gyrokinetic transport solver `TRINITY` with model turbulent fluxes indicate there is an optimal ratio of external torque to power for confinement (arising due to subcritical turbulence driven at large flow shearing rates). This optimal ratio is dependent on the beam power, decreasing towards experimentally obtainable values as power is increased. Further simulations with radially varying current profiles should provide information on the location and radial extent of regions of enhanced temperature gradient. Based on our local gyrokinetic simulation results (as well as previous numerical and experimental evidence), we expect these regions to occur where magnetic shear is low. Extending this work to use fluxes from first-principles turbulence simulations with nonlinear gyrofluid and gyrokinetic solvers is an ongoing project.

Acknowledgements: This work was part funded by the RCUK Energy Programme

under grant EP/G003955 and the European Communities under the contract of Association between EURATOM and CCFE. Travel support was provided by the Leverhulme network for Magnetised Turbulence in Astrophysical and Fusion Plasmas. The views and opinions expressed herein do not necessarily reflect those of the European Commission.

References

[1] K. H. Burrell, Phys. Plasmas **4**, 1499 (1997).

[2] G. D. Conway *et al.*, Phys. Rev. Lett. **84**, 1463 (2000).

[3] R. E. Waltz, G. D. Kerbel, and J. Milovich, Phys. Plasmas **1**, 2229 (1994).

[4] R. E. Waltz, R. L. Dewar, and X. Garbet, Phys. Plasmas **5**, 1784 (1998).

[5] J. E. Kinsey, R. E. Waltz, and J. Candy, Phys. Plasmas **12**, 062302 (2005).

[6] P. J. Catto, M. N. Rosenbluth, and C. S. Liu, Phys. Fluids **16**, 1719 (1973).

[7] A. G. Peeters and C. Angioni, Phys. Plasmas **12**, 072515 (2005).

[8] C. M. Roach *et al.*, Plasma Phys. Control. Fusion **51**, 124020 (2009).

[9] M. Kotschenreuther, G. Rewoldt, and W. M. Tang, Comp. Phys. Comm. **88**, 128 (1995).

[10] A. M. Dimits *et al.*, Phys. Plasmas **7**, 969 (2000).

[11] M. Barnes *et al.*, Phys. Rev. Lett., submitted (2010), arxiv:1007.3390.

[12] E. G. Highcock *et al.*, Phys. Rev. Lett., submitted (2010), arxiv:1008.2305.

[13] R. E. Waltz, G. M. Staebler, J. Candy, and F. L. Hinton, Phys. Plasmas **14**, 122507 (2007).

[14] S. L. Newton, S. C. Cowley, and N. F. Loureiro, Plasma Phys. Control. Fusion, submitted (2010), arXiv:1007.0040.

[15] A. A. Schekochihin, S. C. Cowley, and E. G. Highcock, Plasma Phys. Control. Fusion, submitted (2010).

[16] F. I. Parra *et al.*, Phys. Rev. Lett., submitted (2010), arxiv:1009.0733.

[17] M. Buhmann, Acta Numerica **9**, 1 (2001).

[18] M. Barnes *et al.*, Phys. Plasmas **17**, 056109 (2010), arxiv:0912.1974.

[19] H. Sugama and W. Horton, Phys. Plasmas **4**, 405 (1997).

[20] I. G. Abel *et al.*, Plasma Phys. Control. Fusion, submitted (2010).

[21] P. C. de Vries *et al.*, Plasma Phys. Control. Fusion **48**, 065006 (2008).

[22] G. R. McKee *et al.*, Nucl. Fusion **49**, 115016 (2009).